scientific reports

Check for updates

OPEN

# The dynamics of plant nutation

Vicente Raja[1]✉, Paula L. Silva[2], Roghaieh Holghoomi[3,4] & Paco Calvo[4]

**In this article we advance a cutting-edge methodology for the study of the dynamics of plant movements of nutation. Our approach, unlike customary kinematic analyses of shape, period, or amplitude, is based on three typical signatures of adaptively controlled processes and motions, as reported in the biological and behavioral dynamics literature: harmonicity, predictability, and complexity. We illustrate the application of a dynamical methodology to the bending movements of shoots of common beans (*Phaseolus vulgaris* L.) in two conditions: with and without a support to climb onto. The results herewith reported support the hypothesis that patterns of nutation are influenced by the presence of a support to climb in their vicinity. The methodology is in principle applicable to a whole range of plant movements.**

Since first described extensively by Charles Darwin[1,2], bending movements of nutation have been studied in monocotyledons and dicotyledons[3], in fungi, algae, or bryophytes[4,5], and in shoots and roots of climbing plants[6–10], among others[11–14]. Most kinematic aspects of nutation in different plants species have been thoroughly researched—e.g., oscillatory shapes and directions[15–17], period[18,19], or amplitude[20,21]. Nutation kinematics of different organs has served to lay a foundation of several mechanisms postulated as responsible for the movement in question: internal oscillators[2,20,22], gravitation-driven mechanisms[23,24], or a combination of these two mechanisms[25–27]. Moreover, nutation has been taken to be an instance of plants' adaptively controlled motion[2,27–32]. However, which one of those proposed mechanisms better accounts for the complex kinematics of plant nutation, both generally and in terms of adaptive control, requires experimental adjudication.

Different models inspired by very different assumptions aim to do so. The assumptions of these models range from a purely nastic, non-directional nature of the movement[17] to a full-fledged tropic rendering, including models that resort to kinematical landmarks deployed in the animal literature to characterize directional grasping behavior[33]. All such models nonetheless run the risk of generating the same average kinematical patterns—quasi-circular and quasi-elliptical patterns depending on their parametrization—despite those different assumptions[17,22,23,34–36]. For this reason, current methods based solely on the kinematics of nutation are not helpful in deciding between the different hypotheses regarding the tropic and/or nastic components of plant nutation and their underlying mechanisms. A fundamental step to experimentally discern about these issues is to achieve a more profound understanding of the nature of plant nutation.

The aim of this article is thus to go beyond basic plant kinematics to improve our understanding of plant nutation through a careful characterization of its underlying dynamical organization. To overcome the problems of the approaches based on kinematical patterns, we looked for methods described outside the field of plant science to capture the dynamical processes that give rise to those patterns. These methods, thoroughly used in the behavioral and biological sciences[37–40], are not based on summary statistics or average patterns, blind to the temporal dependencies in the observed movement. Instead, the methods herewith reported are sensitive to such temporal dependencies, offering better access to the underlying dynamical organization that gives rise to them. In this sense, we are not proposing just an alternative description of nutation patterns but a completely novel way to look at them.

Our methodology is based on the analysis of time series gathered by a common procedure in the field—time-lapse, zenithal point-view recording of nutation[7,27,31,41]—and provides measurements for three typical signatures of biologically controlled processes reported in the literature on biological and behavioral dynamics: harmonicity, predictability, and complexity[42–56]. The relationship between these signatures and biologically controlled processes has to do with the temporal dependencies of these processes. As opposed to completely random processes, the states of controlled processes at any moment of time, although variable, are partially determined by their own previous states and by the environmental factors that influence them. The influences of those environmental factors make biologically controlled processes more predictable with respect to them: they tend to re-visit similar states due to those influences. And the combination of variability (randomness) and determinism is the signature of complex processes[46,53,57–61].This is the sense in which the proposed measurements are adequate to study biologically controlled processes.

[1]Rotman Institute of Philosophy, Western University, London, Canada. [2]Department of Psychology, University of Cincinnati, Cincinnati, USA. [3]Department of Biology, Faculty of Science, Urmia University, Urmia, Iran. [4]Minimal Intelligence Lab, University of Murcia, Murcia, Spain. ✉email: vgalian@uwo.ca

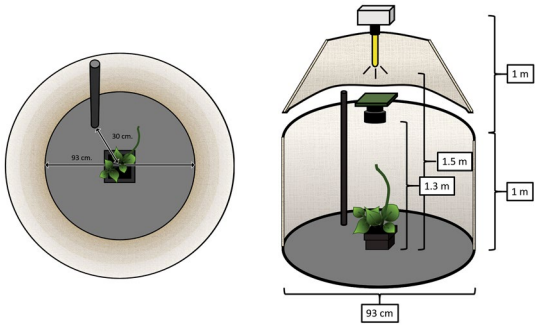


**Figure 1.** Diagram of the experimental setting (see Method for full details). Cylindrical booth for the pole condition. The cylindrical booth for the no-pole condition was identical except for the presence of the pole. Left: Zenithal camera viewpoint of a bean plant and the pole (30 cm away from the bean plant; height: 0.90 m, diameter: 1.8 cm) in the cylindrical boot (width: 93 cm). Right: Lateral viewpoint of a bean plant and the pole in the cylindrical booth. *Time Lapse Camera:* Brinno TLC200 PRO (height: 130 cm); 4.2 µm High Dynamic Range (115 dB) image sensor for recording in darkness. *Illumination:* high-pressure sodium lamp Lumatek pulse-start HPS Lamp 250 W (height: 150 cm; photon fluence rate: 430 ± 50 µmol $m^{-2}$ $s^{-1}$ at leaf level). A white parabolic reflector provided symmetrical lighting.

To illustrate the application of the methodology in the plant sciences, we compared the nutation dynamics of bean plants growing with and without a support (a pole) to twine around in otherwise identical environments. We hypothesized that if nutation patterns were influenced by the presence of sources of perturbation in the vicinity such as the presence of a pole, the plants' bending movements would exhibit a nonlinear organization that would be more predictable and complex when the pole was present. The logic of our study, therefore, consisted in first gathering the proper data to assess the dynamics of plant nutation. Then, we confirmed that nutation patterns were the product of nonlinear processes by using a harmonicity index. Finally, we explored the effect of a pole when present in the vicinity of plants by assessing its influence in the predictability and the complexity of their nutation patterns.

In the rest of the paper, we show how the general methodology was applied in the mentioned study and the way in which the measurement of the dynamical properties of nutation patterns speak to the possible mechanism that controls movement and the influence of the climbing support. Overall, our aim is twofold: (i) to illustrate the use of nonlinear methods to test hypotheses regarding the nature of plant nutation and the environmental factors that might influence it; and (ii) to furnish plant scientists with a set of guidelines for the processing of movements of nutation in a reliable and informative manner.

## Results

The first step of our study was to gather the appropriate time-series data to analyze the dynamical features of nutation patterns. To do so, we designed an experimental analysis on the common bean (*Phaseolus vulgaris* L. var. Bueno Aires) based on established protocols[27]. Concretely, we recorded the behavior of twenty potted common bean plants in two different conditions: with and without a climbing support (a pole) in their vicinity (see Supplementary Video V1 and V2). The twenty plants were placed pairwise in two identical recording cylindrical booths, one pair at a time for a total of ten pairs (Fig. 1). In one of the cabins, a pole was placed 30 cm away from the plant. There was no climbing support in the control recording cabin (see "Methods" section).

Zenithal pictures were taken at one-minute intervals from the onset of plant nutation until the shoot tip of the bean made contact with the pole. Time-lapse footage was assembled out of the zenithal frames being taken (number of frames ranged from 2300 to 5300; M ± SD = 3576.5 ± 842.83). Using the *Circumnutation Tracker (CT)* software[41], the position of each plant's shoot tip in the horizontal plane was digitalized at a 6 Hz rate and time series of the movement that ranged between 451 and 1049 data points (M ± SD = 715.3 ± 168.56) were generated (Fig. 2b; see also Supplementary Data D1). Fast-Fourier transformations showed that most of the frequency power of the movement was concentrated under 0.5 Hz (M ± SD = 0.29 ± 0.05; Fig. 2a). To minimize high frequency noise, a low-pass filter with a cut-off frequency of 1 Hz was used.

To examine the effect of time on nutation dynamics, we divided the data into as many hoping windows of 100 data points as possible, starting from the last point defined by the moment at which the plant in the pole condition touched the pole. For most plants, this procedure guaranteed at least 6 windows of 100 points that were used for analysis. Amplitude and frequency of nutation changed over time, but detailed analysis showed that data was stationary within each window (see "Methods" section and Supplementary Figure F1). Measures of harmonicity, predictability, and complexity of nutation patterns were computed for each plant in each of the six analyzed windows (Windows coded 1 to 6; see Table 1 and Supplementary Data D1).

**Harmonicity of nutation patterns: normalized peak acceleration.** Biologically controlled processes—including movements—are the product of nonlinear dynamics that make them diverge from purely harmonic patterns. In our study, we used Normalized Peak Acceleration (NPA) to quantify such divergence. NPA was computed to assess the degree of deviation of the recorded plant movements from a purely sinusoidal

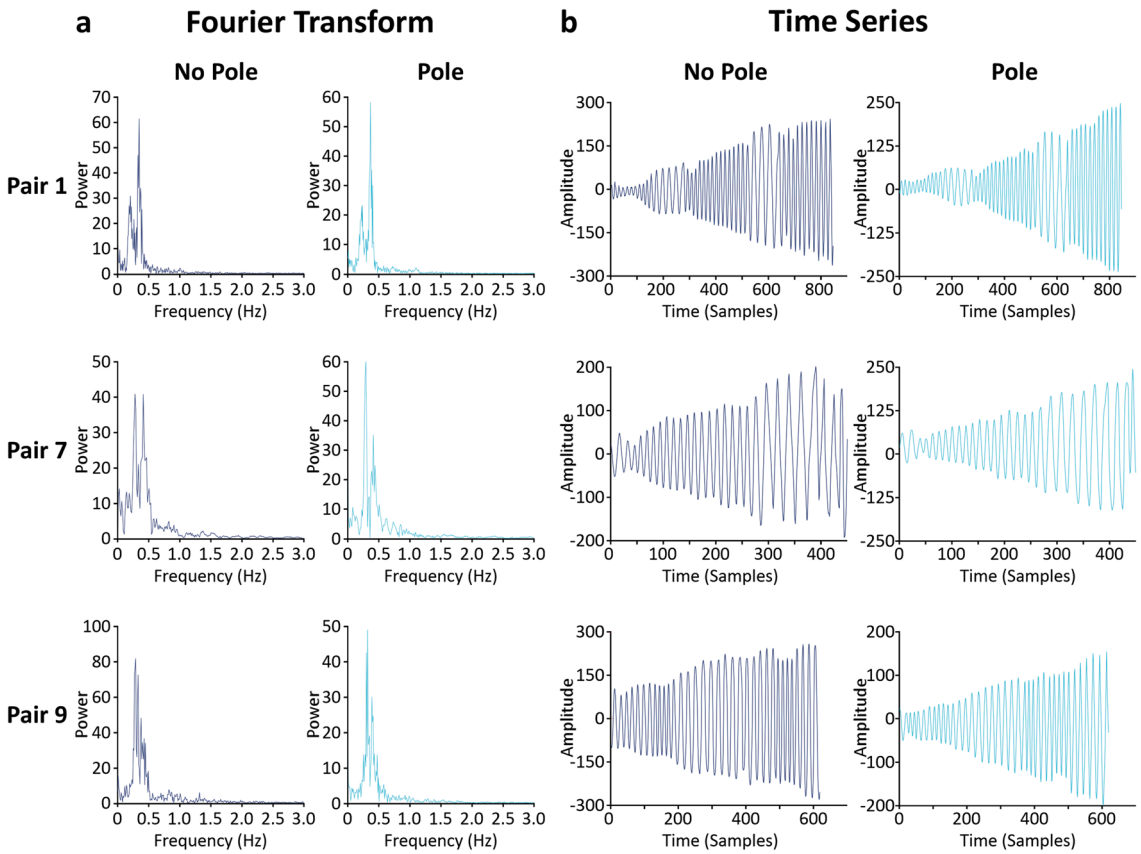


**Figure 2.** Three examples of the detail of the time series (Pair 1, Pair 7, and Pair 9 out of the ten pairs used in the study). Every row corresponds to one pair of plants. (**a**) Fast-Fourier Transformation of the pairs of time series organized by condition. Main frequency components were around 0.15–0.35 Hz for all plants. (**b**) Time-series organized by condition. Displacement of the shoot-tip across the x-axis of the frames. Amplitude of the displacement of the shoot-tip (in pixels) is plotted against time (in samples).

| | | Samples per Window (Range) | | | | | | | | | | |
|---|---|---|---|---|---|---|---|---|---|---|---|---|
| Pair | Total | −4 | −3 | −2 | −1 | 0 | 1 | 2 | 3 | 4 | 5 | 6 |
| 1 | 846 | – | – | 0–45 | 46–145 | 146–245 | 246–345 | 346–445 | 446–545 | 546–645 | 646–745 | 746–846 |
| 2 | 1049 | 0–48 | 49–148 | 149–248 | 249–348 | 349–448 | 449–548 | 549–648 | 649–748 | 749–848 | 849–948 | 949–1049 |
| 3 | 795 | – | – | – | 0–94 | 95–194 | 195–294 | 295–394 | 395–494 | 495–594 | 595–694 | 695–795 |
| 4 | 760 | – | – | – | 0–59 | 60–159 | 160–259 | 260–359 | 360–459 | 460–559 | 560–659 | 660–760 |
| 5 | 655 | – | – | – | – | 0–54 | 55–154 | 155–254 | 255–354 | 355–454 | 455–554 | 555–655 |
| 6 | 750 | – | – | – | 0–49 | 50–149 | 150–249 | 250–349 | 360–449 | 450–549 | 550–649 | 650–750 |
| 7 | 451 | – | – | – | – | – | – | 0–50 | 51–150 | 151–250 | 251–350 | 351–451 |
| 8 | 528 | – | – | – | – | – | 0–27 | 28–127 | 128–227 | 228–327 | 328–427 | 428–528 |
| 9 | 619 | – | – | – | – | 0–18 | 19–118 | 119–218 | 219–318 | 319–418 | 419–518 | 519–619 |
| 10 | 699 | – | – | – | – | 0–98 | 99–198 | 199–298 | 299–398 | 399–498 | 499–598 | 599–699 |

**Table 1.** Window selection for each pair of plants. Hoping windows (100 samples each) are labelled starting from the last window (6) and going backwards from it. The process of selection ensures homogeneity and stationarity of the data in the windows relevant for the analysis (Windows 1 to 6).

(harmonic) pattern. $A\omega^2$ corresponds to the peak acceleration of a sinusoidal movement of amplitude $A$ and frequency $\omega^2$. Thus, a purely sinusoidal movement governed by linear dynamics gives rise to an NPA value of 1. Figure 3a displays the mean (and standard error) of NPA over time for the two conditions. Observed NPA values are larger than 1 and therefore indicate that nutation patterns are not purely sinusoidal or harmonic. These deviations from harmonicity in turn signal the contribution of nonlinear processes to nutation.

Linear mixed effect analysis examined the fixed effect of pole (No Pole = 0, Pole = 1), time (Window = 1 to 6), and their interaction on NPA. The full model also included the random effects of individual plant, plant pair,

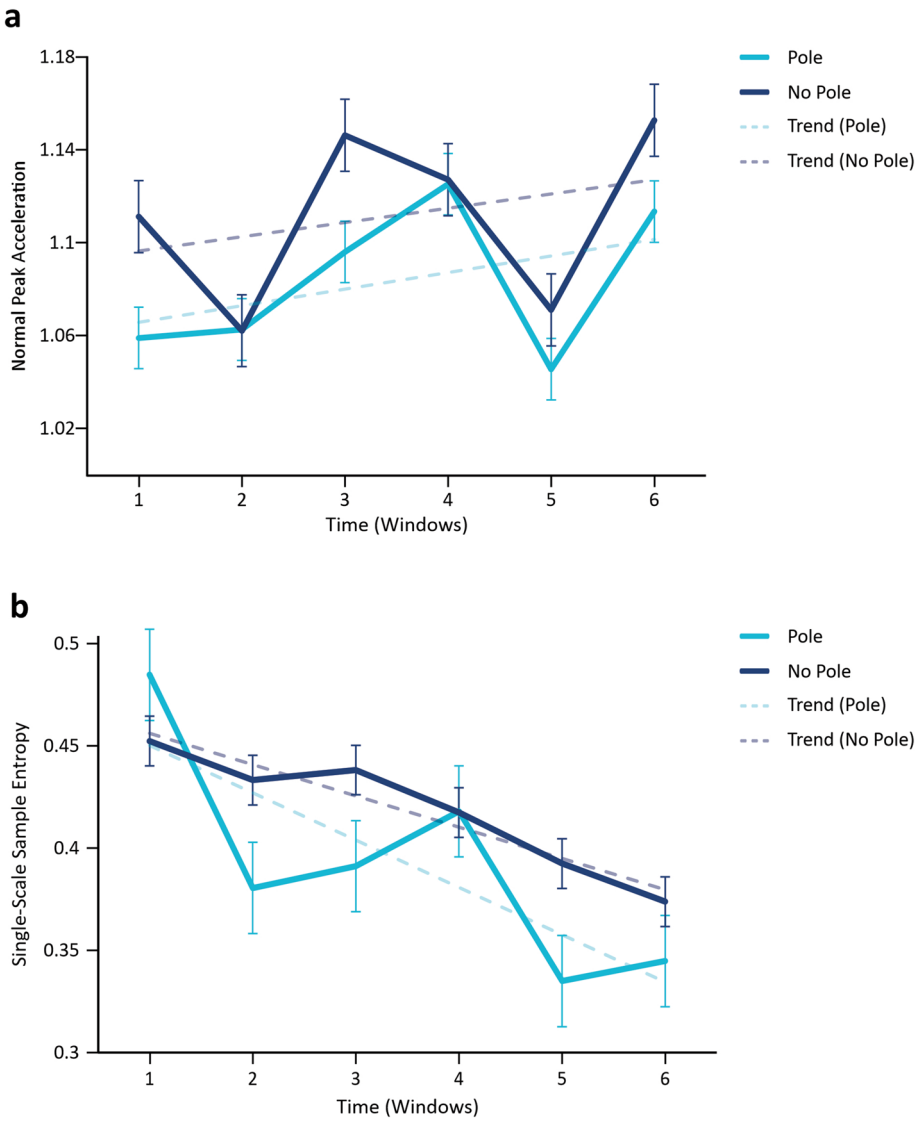


**Figure 3.** Normal peak acceleration (NPA) and sample entropy (SampEn). (**a**) NPA Analysis. Average values of NPA per windows 1 to 6 including standard errors. Solid light blue line plots average NPA values for plants in pole condition and dashed light blue line plots its linear trend. Solid dark blue line plots mean NPA values for plants in no-pole condition and dashed dark blue line plots its linear trend. (**b**) SampEn Analysis. Average SampEn values per windows 1 to 6 and standard errors for $m = 2$, $r = .25$. Solid light blue line plots average SampEn values for plants in pole condition and dashed light blue line plots its linear trend. Solid dark blue line plots average SampEn values for plants in no-pole condition and dashed dark blue line plots its linear trend.

and the nested random effect of time (Window) on NPA. Examination of changes in model fit (-2LL) with stepwise removal of fixed effects revealed no effect of the pole x window interaction ($\chi^2$ (1) = 0, p = 0.99), of the pole ($\chi^2$ (1) = 1.4649, p = 0.23), or of time ($\chi^2$ (1) = 1.402, p = 0.24) on NPA (see Supplementary Data D1 and D2). The average changes in NPA values suggest that the patterns of variation in the kinematics of plant nutation are more complicated than the gradual shift from more circular to more elliptical shapes commonly reported in the literature[7,15,27] (see Fig. 3a). Importantly for present purposes, the changes in kinematics identified by NPA do not capture processes that reflect the potential effect of the pole in the pattern of nutation.

**Predictability of nutation patterns: sample entropy.** The second signature of biologically controlled movements we explored in our study was predictability. When biological movements are controlled, they are controlled *with regard to* relevant environmental factors. For this reason, these movements are more predictable in the presence of those factors. In our study, we used a Sample Entropy (SampEn) analysis to measure the predictability (or regularity) of nutation patterns over time. SampEn constructs vectors of length $m$ out of the data points and then computes the conditional probability of finding matching vectors of length $m+1$ within a tolerance radius $r$ if matching vectors of length $m$ have been already found within that tolerance radius $r$. Lower SampEn values (values closer to 0) indicate more predictability. Figure 3b displays the mean (and standard

| Single-scale sample entropy (SampEn) | | |
|---|---|---|
| **Fixed effects** | **Estimate** | **Standard error (SE)** |
| (Intercept) | 0.502 | 0.035 |
| Condition: pole | − 0.027 | 0.011 |
| Time: window | − 0.023 | 0.005 |
| **Random effects** | **Variance** | **Standard deviation (SD)** |
| Pair (intercept) | 0.002 | 0.049 |
| Nested: window | 0.008 | 0.087 |
| Residual | 0.004 | 0.064 |

**Table 2.** Final model estimated to test the effects of time (Window) and condition (Pole) on SampEn. The model includes all significant fixed effects and all random and nested random effects. Intercept provides an estimate of performance in the base line condition (No Pole = 0). Estimates are the non-standardized weights or coefficients in the linear mixed effect model.

error) of SampEn over time for the two conditions when the length of vectors is $m = 2$ and the tolerance radius is $r = 0.25$. Observed changes in SampEn values in Fig. 3b suggest that nutation patterns become more predicatable in time for both conditions and that nutation is more predictable in the presence of the pole.

To test this observation, we run a linear mixed effect analysis to examine the fixed effect of pole (No Pole = 0, Pole = 1), time (Window = 1 to 6), and their interaction on SampEn. The full model also included random effects of plant pair and the nested effect of time (Window) on SampEn. Examination of changes in model fit (-2LL) with step-wise removal of fixed effects revealed a significant effect of time ($\chi^2$ (1) = 14.973, $p < 0.001$) and a significant effect pole ($\chi^2$ (1) = 4.9049, $p < 0.03$) on SampEn (see Table 2, and Supplementary Data D1 and D2). The interaction between pole and time was not significant. This suggests a progressive increase in predictability of nutation patterns as plants grow, and an influence of the presence of a pole in the vicinity of plants in the overall predictability of the time series. Such an influence is a first indicative of the possible effect of the availability of a support to climb on the patterns of climbing beans' nutation by making them more predictable.

**Complexity of nutation patterns: EMD-based multiscale sample entropy.** The results of the above analysis of the predictability of the climbing beans' nutation patterns suggest that the presence of a pole in their vicinity has an effect in the dynamics of the movements. This kind of effect is usually reflected in its complexity: when the movement is controlled with respect to an environmental factor, it becomes more complex in the presence of that factor. In our study, Multiscale Sample Entropy (MSE) was used to analyze the complexity of nutation patterns; that is, the degree of interactivity of multiscale processes giving rise to nutation. Accordingly, MSE computes SampEn of nutation patterns over time at different temporal scales of the movement. These scales are defined in terms of its intrinsic mode frequencies (IMFs) by a procedure of fine-to-coarse Empirical Mode Decomposition (EMD; see Fig. 4a). Higher irregularity (or higher magnitudes of SampEn) on a single scale can indicate less deterministic structure or a greater degree of randomness in the pattern. Higher irregularity that is preserved across two or more temporal scales, however, suggests greater complexity: a mix of interconnected deterministic and stochastic processes evolving across scales typical of adaptive, biological movements. This is usually reflected in higher and more stable SampEn values across those scales although the SampEn value of the first scale—the whole signal—may be higher for the least complex data[46–48,53–56]. Consistent with MSE literature, average SampEn values across scales of analysis in Fig. 4b suggest that the irregularity of nutation patterns is slightly higher for the no pole condition at scale 1 (left chart). The irregularity of nutation patterns and its associated SampEn values progressively become higher and more stable in subsequent scales for the plants in the pole condition for at least some windows of time (right chart).

To test this observation, we ran a linear mixed effect analysis to examine the fixed effects of pole (No Pole = 0, Pole = 1), time (Window = 1 to 6), and temporal scales of analysis (Scale = 1 to 7), in addition to all their interactions on SampEn ($m = 2$, $r = 0.25$). The full model also included the random effect of plant pair along with a nested random effect of time (Window) and the random effect of individual plants along with a nested random effect of scale on SampEn. Removing the pole x window x scale interaction from the model resulted in a significant reduction in fit (-2LL), $\chi^2$ (1) = 5.6645, $p = 0.017$ (see Table 3, Full Model; see also Supplementary Data D1 and D2). A detailed visual analysis of the average changes in SampEn across scales for the different windows in the two conditions (Fig. 4b) guided initial interpretation of this statistically significant three-way interaction. In particular, we observe that the overall reduction in the magnitude of SampEn (i.e., the amount of irregularity in nutation patterns) as we move across temporal scales of analysis follows two different arrangements. Notably, in the no pole condition the magnitude of SampEn is not preserved across any of the temporal scales of analysis. In contrast, when the pole is present the magnitude of SampEn is preserved across scales 2 and 3 for windows 3, 4, and 6. This is a signature of the complex structure in the variability of those patterns at those stages of the movement (Windows = 3, 4, and 6) and at temporal scales (Scale 2–0.1 Hz, and Scale 3–0.05 Hz) that capture a relevant part of the frequency power of the signal (see Fig. 4a).

To determine whether these observed arrangements were statistically reliable, we ran a linear mixed effect analysis to examine the changes of SampEn values for the two conditions (No Pole = 0, Pole = 1) focusing in scales 2 and 3 and windows 3, 4, and 6. The model included the random effect of plant pair and the nested effect of time (Window). Removing the pole x scale interaction effect from the model resulted in a significant reduction of fit

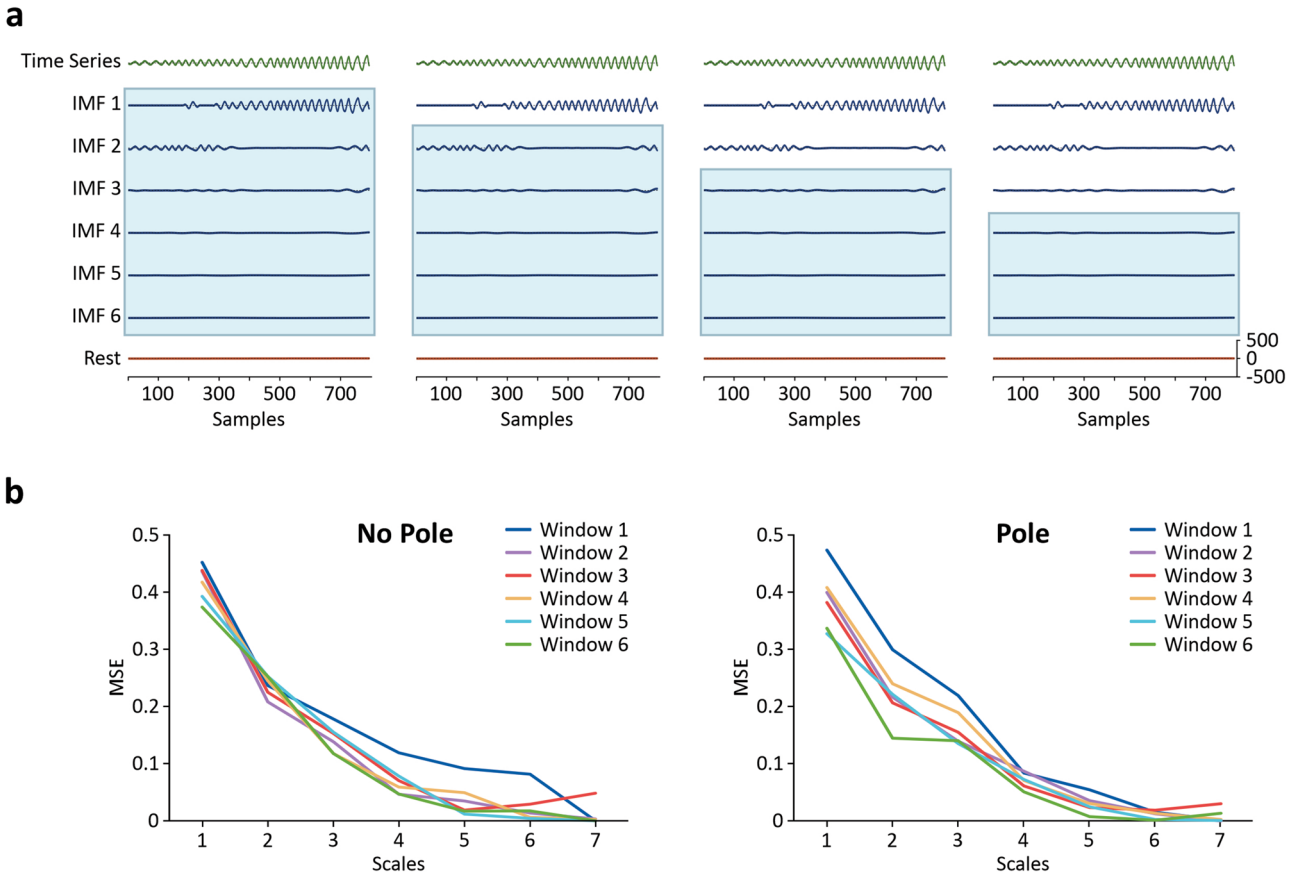


**Figure 4.** Empirical Mode Decomposition and Multiscale Sample Entropy. (**a**) Example of EMD analysis of a time series and of the fine-to-coarse EMD procedure. The 4 panels show the EMD for the Pair 3, pole condition plant (see Table 1). From top to bottom, each panel shows: full time series (green), six IMFs (blue), and Rest of signal (red). Light blue squares show IMFs that are included in each Scale generated by a fine-to-coarse EMD procedure. Left panel represents Scale 1 including IMFs 1 to 6 (the whole signal). Second to left panel represents Scale 2 including IMFs 2 to 6 after subtracting the highest frequency component (IMF 1). Second to right panel represents Scale 3 including IMFs 3 to 6 after subtracting the two highest frequency components (IMFs 1 and 2). Right panel represents Scale 4 including IMFs 4 to 6 after subtracting the three highest frequency components (IMFs 1, 2, and 3). (**b**) EMD-based MSE ($m = 2$, $r = .25$) for all windows and scales. Left chart shows no-pole condition. Right chart shows pole condition. General reduction of the average magnitude of SampEn is observed for both conditions. The average magnitude of SampEn is preserved across scales 2 and 3 for windows 3, 4, and 6 in pole condition.

(-2LL), $\chi^2$ (1) = 4.3589, $p < 0.04$ (see Table 3, Focused Model; see Supplementary Data D1 and D2). Follow-up analyses of variance showed that average SampEn values were significantly reduced from scale 2 to scale 3 in windows 3, 4, and 6 for the no-pole condition ($F(1, 4) = 60.69$, $p = 0.001$), but not for the pole condition ($F(1, 4) = 1.28$, $p = 0.32$), confirming the arrangements observed in Fig. 4b (see Supplementary Data D1 and D2). Subsequent MSE analysis of the surrogate shuffled time series of the plants in the pole condition showed the vanishing of the arrangement observed in Fig. 4b and, therefore, offered further support to the presence of a complex structure in the variability of nutation patterns in windows 3, 4, and 6 (see Supplementary Figure F1). In conjunction, these results show that when a climbable structure is present in the plants' environment, the variability in nutation patterns is more complex, that is, structured by a blend of deterministic and random processes. Such results constitute further evidence for the possible effect of the availability of a support to climb on the patterns of climbing beans' nutation.

## Discussion

One aim of our study was methodological: for the first time in the literature, we applied nonlinear methods of behavioral analysis to the dynamics of plant nutation. The direct study of the dynamical features of plant nutation provides a way to understand the movement beyond its kinematical characteristics. The study of the kinematics of nutation usually requires a two-dimensional[7] or even a three-dimensional[17] analysis to reach an understanding of the movement that is allegedly able to shed light on its underlying mechanism[15,17,22]. However, we have shown that there are methods to assess dynamical features of plant nutation from a one-dimensional time-series describing the movement over time—as it is commonly acknowledged in the sciences of complexity[43,57,62]. Indeed, the proposed methodology allows for a direct and complete study of the dynamics of plant nutation without

| Multiscale sample entropy (MSE) | | | |
|---|---|---|---|
| **Full model** | | **Focused model** | |
| **Fixed effects** | **Estimate (SE)** | **Fixed effects** | **Estimate (SE)** |
| (Intercept) | 0.436 (0.029) | (Intercept) | 0.501 (0.074) |
| Condition: pole | 0.083 (0.028) | Condition: Pole | −0.188 (0.09) |
| Time: window | −0.007 (0.005) | Time: window | −0.009 (0.008) |
| Scale | −0.08 (0.009) | Scale | −0.111 (0.025) |
| Pole*window | −0.026 (0.007) | Pole*scale | 0.075 (0.035) |
| Pole*scale | −0.009 (0.009) | | |
| Window*scale | 0.001 (0.001) | | |
| Pole*window*scale | 0.004 (0.002) | | |
| **Random effects** | **Variance (SD)** | **Random effects** | **Variance (SD)** |
| Pair (intercept) | 0.005 (0.068) | Pair (intercept) | 0.0004 (002) |
| Nested: window | 0.0004 (0.02) | Nested: window | 0.001 (0.03) |
| Plant (intercept) | 0.00009 (0.009) | Residual | 0.009 (0.097) |
| Nested: scale | 0.0005 (0.022) | | |
| Residual | 0.004 (0.064) | | |

**Table 3.** Final models estimated to test the effects of time (Window) and condition (Pole) on SampEn at the different temporal scales of analysis generated by a fine-to-coarse EMD procedure (Scale). Left panel: Full model including all windows and scales. Right panel: focused model including windows 3, 4, and 6, and scales 2 and 3. Both models include all significant higher-order interactions, all lower-order interactions, all component lower-order effects, and all random and nested random effects. Interactions are marked by '*'. Intercept provides an estimate of performance in the base line condition (No pole = 0). Estimates are the non-standardized weights or coefficients in the linear mixed effect model.

relying on particular kinematic patterns or ad hoc modelling criteria (e.g., modeling climbing plants' grasping of a support in terms of hypothetical animal wrist-like and digit-like—thumb and index—ensembles)[33]. It is important to note that our methodology frees hypothesis-testing from zoomorphic biases.

Another important aspect of the methodology is that it provides guidelines for plant scientists to process nutation data, and potentially other plant movements, in a reliable and informative way. The methodology (described in detail in the "Methods" section) can be applied to any movement data collected by time-lapse videos from the zenithal point of view and digitalized in the form of time series of data points. This fact, along with the already mentioned parsimony of assumptions, makes the methodology widely applicable. Moreover, the methodology provides justification and procedures for choosing one dimension of the movement, for assessing the frequency-resolution needed to capture the relevant information, for assessing stationarity, for selecting the windowing of the data, and for selecting the parameters of the entropy analyses. In this way, the proposed methodology becomes a basis for the generalization of nonlinear methods of behavioral analysis for plant movements.

When the methodology was applied to the study of common beans' nutation in two conditions (pole vs. no pole), the way dynamical measurements allowed for a deeper understanding of the movement became manifest. Our hypothesis was that, if the presence of a support to climb had an effect in the patterns of nutation, this fact would be reflected in the dynamical properties of the movement. In particular, common beans' nutation with a support to climb in their surroundings would exhibit common signatures of biologically controlled processes in terms of harmonicity, predictability, and complexity. The results of our study show these three signatures in nutation, strongly suggesting that the support to climb is to be regarded as a relevant environmental factor for the biological control of nutation.

This result speaks to the mechanism of nutation and its relationship to the kinematics of the movement. First, the results of the analysis of harmonicity show that the commonly reported gradual shift from more circular to more elliptical shapes in the nutation patterns of climbing beans is actually a non-gradual, elaborate shift and is not related to the possible adaptive processes that guide plants towards a support to climb. And second, the differences found both in single-scale and multiscale sample entropy for the two conditions suggest that a mechanism based on endogenous, purely linear oscillators[2,17,20,22] are not good enough to capture the complexity of nutation in different environmental settings. Instead, a mechanism that is not merely influenced by endogenous factors, and that is sensitive to the position of a support to climb in the environment of the plant, proves to be a better candidate.

Last, the complexity shown by nutation patterns in our study when a support to climb was present in the surroundings of the plants is compatible with the finding that complexity in plants' electrical signaling may be driven by external factors[63]. More research is needed to fully understand nutation dynamics and to corroborate different aspects of their tropic components—e.g., exploring nutation in other plants, modelling nutation both at the behavioral and cellular scales, etc.—and the seemingly intermittent influence of the support to climb onto. These may be due to other conditions intermittently affecting the movement; conditions whose identification calls for the development of yet further experimental designs. Overall, the proposed methodology, formed by three different measurements of movement dynamics, constitutes a robust tool to pursue this kind of research.

With this methodology, plant scientists can improve the understanding of the dynamics of plant movements and gain perspective with regard to the fundamental features and underlying mechanisms of plant nutation.

## Methods

**Plant materials.** Experiments were performed with the common bean (*Phaseolus vulgaris* L.). Seeds of the cultivar "Buenos Aires" were provided by Semillas Ramiro Arnedo S.A., Spain https://www.ramiroarnedo.com.

**Germination and growth conditions.** Plants were light-grown from seed in a controlled-environment chamber (300 × 400 × 240 cm.) at the Minimal Intelligence Lab (MINT Lab), University of Murcia, Spain.

Prior to sowing, Buenos Aires var. common bean seeds were germinated on filter paper, soaked in an aqueous solution of hydrogen peroxide ($H_2O_2$)—15 mL distilled water/3 mL $H_2O_2$—to promote germination in Petri dishes kept in darkness for 24–48 h. Upon germination, young seedlings were transferred to coconut fiber growing pellets and kept on propagation trays. Humidity levels were checked periodically to maintain a moist bedding.

Once the first pair of true leaves had appeared, healthy-looking seedlings were transplanted into a mixture of peat moss and perlite (70–30%) in the center of small black plastic pots (70 × 70 × 80 mm. in depth). The temperature of the growth chamber was kept on a 23 °C (day) and 19 °C (night) ± 1 °C, photoperiod at L16:D8 h. light cycle, and relative humidity 55% ± 5%. Light was delivered from the top (photosynthetically active radiation (PAR) photon fluence rate of 235 ± 25 µmol $m^{-2}$ $s^{-1}$ at leaf level—Delta OHM HD 9021 solid state PAR sensor, Caselle di Selvazzano (PD), Italy).

Plants were watered (filtered tap) two hours into the photoperiod. All seedlings received the same amount of water per day; amount that progressively increased with plant age from 20 to 60 mL. No other treatment was applied.

**Stimulus and experimental design.** Measurements were carried out from the onset of 'bending': a morphological feature characteristically displayed in *P. vulgaris* as the apical segment below the horizontal section of the shoot apex in ca. two-week-old plants becomes curved[15].

Plants were pairwise compared with an eye to selecting the most similar seedlings as model plant pairs, prior to transfer to the recording booths. Pairwise comparisons were based on uniformity in stem and internode length and diameter, leaf shape and total leaf area. The most uniform subjects that were ready to be transferred into the recording booths were selected. These were transplanted to larger pots (Air Max 7 L square plant pots—200 × 200 × 270 mm in depth) filled with the same mix (70% peat moss/30% perlite). Potted plants were saturated with filtered tap water, and allowed to drain, to avoid any further watering during time-lapse recordings. Pilot tests[31] confirmed that humidity levels could be kept within an optimal range for the duration of the experiment.

Ten pairs of potted plants (20 plants in total) were then randomly allocated, each pair at a time, to two cylindrical booths within the growing chamber, where each plant was placed at the center of a bottom cylinder. Booths were identical with the exception of a vertical pole (height: 0.90 m; diameter: 1.8 cm.) presented as a stimulus—a potential support for the bean to twine around—in only one of the two booths. The pole was placed at a distance of 30 cm from the plant center. Before starting recordings, plants were allowed to stabilize for 2 h after having been transferred.

Each booth consisted of a right circular cylinder with a radius of 93 cm. A height of two meters of the vertical cylindrical surfaces, together with the disposition of the booths within the growth chamber, was such that it prevented air circulation produced by the chamber's extractor (RVK 1000 $m^3$/h) and injector (PK150-L 780 $m^3$/h) used for air renewal and temperature regulation from affecting plants' nutation. To distribute light more uniformly, controlling thereby for light-related factors other than the presence of the pole in the vicinity of the plant, the cylindrical surfaces were covered in white reflective film.

The light source consisted of a high-pressure sodium lamp (Lumatek pulse-start HPS Lamp 250 W) with specific horticultural gas blend for optimal spectral output consistency and PAR/PPF level maintenance for plant growth. Symmetrical lighting was ensured by suspending lamps vertically within the cylindrical booths under a white parabolic reflector. Lamps were positioned centered at 150 cm above each potted plant, providing a photon fluence rate of 430 ± 50 µmol $m^{-2}$ $s^{-1}$ at leaf level.

**Video recording.** Time-lapse cameras (Brinno TLC200 PRO) were placed within each booth 130 cm. off the ground, pointing vertically down to the center of the potted plant. Time-lapse records were made, the time interval between frames for data collection of the position of the shoot tip at one frame per minute. A 4.2 µm High Dynamic Range (115 dB) image sensor made time-lapse recording possible during the 8 h of darkness under a dim phototropically inactive green safelight with a fluence rate under 5 µmol $m^{-2}$ $s^{-1}$. The bottom face of the cylinder was covered in black to maximize the contrast between the shoot tip and the background whilst recording.

**Data processing.** The first processing step is to digitize the 2D coordinates of shoot tips obtained from time-lapse videos. This procedure introduces noise in the time-series, which can be minimized if the selected level of resolution is not too high considering the rate of change in the position of shoot tips. To that end, we digitized the time-lapse videos using resolutions of 24 Hz, 6 Hz, and 3 Hz, and computed the spectral properties of the resulting three time-series using Fast-Fourier transformations. The transformations showed that the fundamental frequencies of the movement were concentrated under 0.5 Hz (M ± SD = 0.29 ± 0.05; Fig. 2a above) for the three tested frequencies, ensuring the robustness of our digitalization process. We subsequently selected the central resolution value, 6 Hz. This choice guarantees that the resulting 2D time-series of the plants' shoot

tips include the relevant information about the nutation movement while avoiding meaningless noise. It also guarantees long enough time series for dynamical analysis.

In line with the literature on dynamics, we assume that the underlying dynamical organization of biological rhythmic movements can be appropriately reconstructed from a single measurement of the behavior of interest[62]. Thus, for all the analyses described below, we have only used the digitalized position time-series of the plants' shoot-tips in the horizontal axis of the video frames.

**Stationarity testing.** Two of the three dynamical analyses used in the present study (*Harmonicity* and *Single-Scale Sample Entropy*) assume stationarity of time-series data. To test this assumption, we initially applied a Dickey–Fuller test (ADF Test)[64]. This test examines the null hypothesis that a unit root—i.e., a stochastic or unpredictable trend or random walk drift in a time-series—is present in a time series sample. If a unit root is not found in a time series, there are no grounds for rejecting the null hypothesis, and stationarity is concluded[65]. We selected this test because of its clear interpretative cut-off to distinguish between stationary and non-stationary data. However, the ADF test suffers from low statistical power and can only exclude strong violations. As a countermeasure to this limitation, we employed a two-step procedure to determine whether weaker violations of stationarity were at play or not[56]. The first step consists in applying transformations to the data to *make them* stationary. These transformations involve either differencing the time-series or fitting a polynomial function and subtracting the fitted trend from the data. The latter transformation is known as detrending or de-seasoning, depending on the way the polynomial function is subtracted from the original time series[66,67]. The second step consists in applying the analyses that assume non-stationarity to both the original and the transformed data, and comparing the results. If results are indifferent to the transformation, it is further evidence that the assumption of stationarity is not being violated (see Supplementary Fig. 1a and b). These methods, however, entail a manipulation of the data that might cause the discarding of important information of the time series, so they must be used carefully.

**Window selection.** To examine whether the effect of the pole on nutation dynamics changes over time, we parsed the data into time-windows. We used a method for window selection that accomplishes two critical goals. First, each window must include enough data points to reveal the underlying dynamical organization of nutation patterns. A good rule of thumb for the analyses employed here is a minimum of 100 data points. And second, windows must not include many overt variations in amplitude and frequency that can impact the results of the dynamical analysis. Accordingly, we selected hoping windows of 100 data points (~ 8 h of movement given our data sampling), starting from the last point defined by the moment at which the plant in the pole condition touched the pole. For most plants, this procedure guaranteed at least 6 windows of 100 points that could be used for the analysis. These relatively small windows prevented large variance in the amplitude and frequency of the time series within the windows while providing enough data points for the dynamical analyses—bigger windows would have resulted in an increase in the risk of violating the stationarity assumption; smaller windows would have compromised the three proposed analyses. However, insofar as nutation patterns can vary dramatically across plant species, our methodological recommendations must be read in terms of criteria for window selection and not in terms of the particular window size herewith selected for the purpose of our analysis.

**Data analysis.** Measures of harmonicity (Normal Peak Acceleration; *NPA* hereafter), regularity (Single-Scale Sample Entropy; *SampEn* hereafter), and complexity (Multiscale Sample Entropy; *MSE* hereafter) of nutation patterns were computed for each plant in each of the six analyzed windows. The analyses performed to compute each of these measures will be described in turn.

**NPA.** The Fast-Fourier transformation (FFT) of the position time-series performed during *Data Processing* (see above) indicated that 99% of the power in the nutation signals was under 1 Hz. Thus, to minimize the influence of noise in the computation of *NPA*, all time-series were filtered using a dual-pass second-order Butterworth filter with a cut-off frequency of 1 Hz. After filtering, the harmonicity of nutation patterns was computed based on the average of the peak acceleration values obtained for each half-cycle[68]. For a purely sinusoidal (or harmonic) movement of amplitude A and frequency ω, peak acceleration is equal to $A\omega^2$. *NPA* was computed by dividing the observed peak acceleration by $A\omega^2$ and is, thus, a sensitive measure of the degree of harmonicity. An *NPA* of 1 is a signature of harmonic patterns, consistent with purely linear control processes. Deviations of *NPA* from 1 index a departure from a purely harmonic pattern, signaling contributions of non-linear processes to the movement of nutation. In order to generate consistent representations of NPA values, NPA values under 1 were regularized using the formula 2—NPA value.

**SampEn.** Generally speaking, different entropy measurements of time series (e.g., Kolmogorov–Sinai entropy, approximate entropy, *SampEn*) aim to assess the probability of knowing future states of the series given measurements of their current states: the more predictable (or regular) the time series is, the lower entropy it has, and vice versa[49,69]. In the case of *SampEn*, such an assessment is pursued in a way inspired by approximate entropy[50]. The general method of *SampEn* consists of the comparison of vectors of different length, $m$ (e.g., $m = 1$, $m = 2$, $m = 3$, and so on), given a tolerance for assessing similarity, $r$. For example, vectors $m = 2$ or $m = 3$ are those composed of 2 or 3 data points of the time series respectively. And a tolerance of $r = 0.25$ defines how much different two vectors can be so as to be deemed similar to one another. The method of *SampEn* calculates the conditional probability of finding a match for a vector of $m + 1$ data points given that it has already found a match for a particular (template) vector of $m$ points[46,57] within a tolerance radius $r$.

In terms of its two parameters, literature on *SampEn* recommends vector lengths of $m = 1$ or 2 and tolerance radiuses, $r$, between 0.1 and 0.25 of the standard deviation of the time series[57]. However, given the properties of the time series of plant nutation, especially its temporal scale (i.e., small displacements from data point to data point) and the general homogeneity of the movement, it might make sense to consider longer vectors (e.g., $m = 3$) than those considered in faster, more variable human/animal movements. Also, different data driven methods of parameter selection have been recently proposed like, for example, the calculation of parameters that relies on autoregression functions of time series[51]. Another option is to estimate the parameter $m$ for a time series by plotting the median *SampEn* values of the time series for several $m$'s as a function of different values of $r$ and then selecting the $m$ or $m$'s at which the curves of *SampEn* values converge, as such convergence is an indicative of having found the $m$/$m$'s that better capture global properties of the time-series[52]. In the case of parameter $r$, the relative error of *SampEn* is calculated and plotted against $r$ values[52]. The $r$ value at which relative error is minimal should be chosen for the analysis. We employed these methods for parameter selection in this study and results suggest that, as a general rule, $m = 2$ or 3 and $r = 0.25$ are reasonable selections. For all the SampEn analyses in this study we used the *Sample Entropy Estimation* package[70] as available in *PhysioNet*[71].

**MSE.** Higher values of *SampEn* (i.e., a measure of reduced regularity) have been interpreted to indicate greater complexity in movement patterns[51,52,56]. However, this is problematic because its value is maximized (around 2) for completely random, unstructured patterns. Such a lack of correspondence may lead to situations in which less complex time series get higher *SampEn* values than more complex ones[53–55]. Complex patterns are characterized by structured variations (i.e. subtle time correlations) in the midst of randomness, reflecting the adaptability (or context sensitivity) of biological patterns[44,58–61]. Importantly, this rich mix of order (regularity) and disorder is preserved across scales when the pattern is complex[47,53,54,72–74].

*MSE* assesses the degree of disorder (*SampEn*) in multiple scales and allows assessment of the extent to which it is preserved across scales. Thus, an *MSE* analysis provides a way to disambiguate between random and complex patterns[44,53]. In particular, at a more microscopic scale, the non-complex time series (e.g., white noise) have a higher *SampEn* value. However, more complex time series exhibit higher and, more importantly, more stable values of *SampEn* at progressively more macroscopic scales (at least in the relevant scales where structure exists). For non-complex patterns, an exponential decrease in *SampEn* is observed as the scale of analysis is increased.

Performing *MSE* analyses requires making a decision regarding the way the different spatiotemporal scales are defined. A "coarse-graining" method in which different scales are generated by averaging the data points of the time series within non-overlapping windows of increasing length—e.g., averaging data points in groups of 2 points, 3 points, 4 points, etc.—has been proposed[44,53]. However, this method has the problem of shortening the time series to a half, to a third, to a quarter, and so on, as the windows of data points increase in length. For this reason, it is not adequate in the case of regular or short time series. We employed instead an empirical mode decomposition analysis (*EMD*) to carve out the relevant spatiotemporal scales of the time series of nutation[48]. In this study we used the EMD MATLAB code available at[75].

*EMD* is a data driven methodology that consists in finding the intrinsic frequency modes (*IFM*) of time series and combining them to generate the different scales. Once these modes are found, there are two ways to perform an *EMD*: (i) coarse-to-fine *EMD*, in which the lowest-frequency *IMF* is subtracted from the signal in each step until only one *IMF* is left; and (ii) fine-to-coarse *EMD*, in which the highest-frequency *IMF* is subtracted from the signal in each step until only one *IMF* is left. Usually, most of the power of the signal in time-series of plant nutation is in the highest-frequency ones, so a fine-to-coarse *EMD* is recommended to get a better understanding of the significant differences between scales.

Finally, to confirm that the complexity observed in *MSE* analyses was not due to an artifact of the analysis, we compared the *MSE* analysis of original time series with the *MSE* analysis of their corresponding surrogate shuffled time series. Shuffling (i.e., randomly reordering) the original time series destroys their temporal dependencies while preserving their statistical features. Therefore, surrogate shuffled time series are by definition less complex than the original time series and the features associated with complexity (e.g., the stability of *SampEn* values across relevant scales) in their *MSE* analysis must vanish if they are not an artifact.

**Statistical analysis.** We used the *lme4* package[76] of the *R Studio*[77] suite to estimate linear mixed effect regression models to examine the contributions of the pole (No pole = 0, Pole = 1), time (Windows 1 to 6), and their interaction to three outcome measures computed to characterize three aspects of plant dynamics: non-linearity, predictability (regularity), and complexity. When modeling complexity, we additionally examined the effect of the temporal scale of analysis (Scales 1 to 7) and its interactions with pole and time. In all cases, we started by identifying the random effects of plant pairs and of the individual plants that should be included in the model. Null models with different combinations of random effects were systematically estimated and the most conservative, best fitting model that converged was selected. We then implemented a backwards approach to identify statistically meaningful fixed effects. The full model included the fixed effects of time, pole, and scale (when pertinent), and their interactions in addition to the random effects previously identified. Models were trimmed by removing fixed effects individually, starting from the higher-order interaction effect. At each step, we compared the deviance (−2 Log Likelihood or −2LL) between a larger model and a simpler nested model that excluded the predictor under analysis. The change in −2LL follows a chi-square distribution with degrees of freedom equal to the difference in the number of parameters between nested models, allowing for a test of statistical significance of each fixed effect. Final models included only significant higher-order interactions, all lower-order interactions, and all component lower-order effects.

## Data availability

All datasets generated or analysed during this study plus 2 sample videos are included in this published article (and its Supplementary Information files). The rest of videos used in the current study are available from the corresponding author on reasonable request.

Received: 29 May 2020; Accepted: 29 October 2020
Published online: 10 November 2020

## References

1. Darwin, C. A. *The Movements and Habits of Climbing Plants* (Murray, Sydney, 1875).
2. Darwin, C. A. & Darwin, F. *The Power of Movement in Plants* (Murray, Sydney, 1880).
3. Baillaud, L. Les mouvements d'exploration et d'enroulement des plantes volubiles. In *Handbuch der Pflanzenphysiologie* (eds Aletsee, L. *et al.*) 637–715 (Springer, Berlin, 1962).
4. Millet, B., Melin, D. & Badot, P.-M. Circumnutation in *Phaseolus vulgaris*. I. Growth, osmotic potential and cell ultrastructure in the free-moving part of the shoot. *Physiol. Plant.* **72**, 133–138 (1988).
5. Badot, P.-M., Melin, D. & Garrec, J. P. Circumnutation in *Phaseolus vulgaris* L. II. Potassium content in the free-moving part of the shoot. *Plant Physiol. Biochem.* **28**, 123–130 (1990).
6. Caré, A. F., Nefedev, L., Bonnet, B., Millet, B. & Badot, P.-M. Cell elongation and revolving movement in *Phaseolus vulgaris* L. twining shoots. *Plant Cell Physiol.* **39**, 914–921 (1998).
7. Mugnai, S., Azzarello, E., Masi, E., Pandolfi, C. & Mancuso, S. Nutation in plants. In *Rhythms in Plants* (eds Mancuso, S. & Shabala, S.) 19–34 (Springer, Berlin, 2015).
8. Brown, A. H. Circumnutations: from Darwin to space flights. *Plant Physiol.* **101**, 345–348 (1993).
9. Kern, V. D. *et al.* Gravitropic moss cells default to spiral growth on the clinostat and in microgravity during spaceflight. *Planta* **221**, 149–157 (2005).
10. Kim, G. H., Yoon, M. & Klotchkova, T. A. A moving mat: phototaxis in the filamentous green algae Spirogyra (Chlorophyta, Zygnemataceae). *J. Phycol.* **41**, 232–237 (2005).
11. Migliaccio, F., Fortunati, A. & Tassone, P. Arabidopsis root growth movements and their symmetry: progress and problems arising from recent work. *Plant Signal Behav.* **4**, 183–190 (2009).
12. Buda, A., Zawadzki, T., Krupa, M., Stolarz, M. & Okulski, W. Daily and infradian rhythms of circumnutation intensity in *Helianthus annuus*. *Physiol. Plant.* **119**, 582–589 (2003).
13. Hayashi, Y. *et al.* An aluminum influence on root circumnutation in dark revealed by a new super-harp (high-gain avalanche rushing amorphous photoconductor) camera. *Plant Cell Physiol.* **45**, 351–356 (2004).
14. Johnsson, A., Solheim, B. G. B. & Iversen, T. H. Gravity amplifies and microgravity decreases circumnutations in *Arabidopsis thaliana* stems: results from a space experiment. *New Phytol.* **18**, 621–629 (2009).
15. Millet, B. & Badot, P.-M. The revolving movement mechanism in Phaseolus. New Approaches to old questions. In *Vistas on Biorhythmicity* (eds Greppin, H. *et al.*) 77–98 (University of Geneva Press, Geneva, 1996).
16. Schuster, J. & Engelmann, W. Circumnutations of *Arabidopsis thaliana* seedlings. *Biol. Rhythm Res.* **28**, 422–444 (1997).
17. Bastien, R. & Meroz, Y. The kinematics of plant nutation reveals a simple relation between curvature and the orientation of differential growth. *PLoS Comput. Biol.* **12**, e1005238. https://doi.org/10.1371/journal.pcbi.1005238 (2016).
18. Johnsson, A. & Heathcote, D. Experimental evidence and models on circumnutations. *Z. Pflanzenphysiol.* **70**, 371–405 (1973).
19. Shabala, S. N. & Newman, I. A. Proton and calcium flux oscillations in the elongation region correlate with root nutation. *Physiol. Plant.* **100**, 917–926 (1997).
20. Brown, A. H., Chapman, D. K., Lewis, R. F. & Venditti, A. L. Circumnutations of sunflower hypocotyls in satellite orbit. *Plant Physiol.* **94**, 233–238 (1990).
21. Hejnowicz, Z. & Sievers, A. Proton efflux from the outer layer of the peduncle of tulip in gravitropism and circumnutation. *Acta Bot.* **108**, 7–13 (1995).
22. Johnsson, A., Jansen, C., Engelmann, W. & Schuster, J. Circumnutations without gravity: a two-oscillator model. *J. Gravit. Physiol.* **6**, 9–12 (1999).
23. Israelsson, D. & Johnsson, A. A theory for circumnutations in *Helianthus annuus*. *Physiol. Plant.* **20**, 957–976 (1967).
24. Johnsson, A. & Israelsson, D. Application of theory for circumnutations to geotropic movements. *Physiol. Plant.* **21**, 282–291 (1968).
25. Johnsson, A. Circumnutations: results from recent experiments on Earth and in space. *Planta* **203**, 147–158 (1997).
26. Orbovic, V. & Poff, K. L. Interaction of light and gravitropism with nutation of hypocotyls of *Arabidopsis thaliana* seedlings. *Plant Growth Regul.* **23**, 141–146 (1997).
27. Stolarz, M. Circumnutation as a visible plant action and reaction. *Plant Signal Behav.* **4**, 380–387 (2009).
28. Larson, K. Circumnutation behavior of an exotic honeysuckle vine and its native congener: influence on clonal mobility. *Am. J. Bot.* **87**, 533–538 (2000).
29. Mancuso, S. & Shabala, S. *Rhythms in Plant* (Springer, Berlin, 2015).
30. Calvo, P. & Friston, K. Predicting green: really radical (plant) predictive processing. *J. R. Soc. Interface* **14**, 20170096. https://doi.org/10.1098/rsif.2017.0096 (2017).
31. Calvo, P., Raja, V., & Lee, D. Guidance of circumnutation of climbing bean stems: an ecological exploration. Preprint (2017).https://doi.org/10.1101/122358.
32. Trewavas, A. The foundations of plant intelligence. *Interface Focus* **7**, 20160098. https://doi.org/10.1098/rsfs.2016.0098 (2017).
33. Guerra, S. *et al.* Flexible control movement in plants. *Sci. Rep.* **9**, 16570. https://doi.org/10.1038/s41598-019-53118-0 (2019).
34. Yoshihara, T. & Iino, M. Circumnutation and rice coleoptiles: its relationship with gravitropism and absence in lazy mutants. *Plant Cell Environ* **29**, 778–792 (2006).
35. Bastien, R., Douady, S. & Moulia, B. A unifying model of plant shoot gravitropism with an explicit account of the effects of growth. *Front. Plant Sci.* **5**, 136. https://doi.org/10.3389/fpls.2014.00136 (2014).
36. Bastien, R., Douady, S. & Moulia, B. A unified model of shoot tropism in plants: photo-, gravi-, and proprioception. *PLoS Comput. Biol.* **11**, e1004037. https://doi.org/10.1371/journal.pcbi.1004037 (2015).
37. Carello, C. & Moreno, M. A. Why nonlinear methods? in *Tutorials in Contemporary Nonlinear Methods for the Behavioral Sciences* (eds. Riley, M. A. & Van Orden, G. C.) 1–25; https://www.nsf.gov/sbe/bcs/pac/nmbs/nmbs.jsp (2005).
38. Holden, J., Riley, M. A., Gao, J. & Torre, K. Fractal analyses: statistical and methodological innovations and best practices. *Front. Psychol.* **4**, 201300097. https://doi.org/10.3389/fphys.2013.00097 (2013).
39. Dotov, D. G., Nie, L. & Chemero, A. A demonstration of the transition from ready-to-hand to unready-to-hand. *PLoS ONE* **5**, e9433. https://doi.org/10.1371/journal.pone.0009433 (2010).
40. Cavanaugh, J. T., Guskiewicz, K. M. & Stergiou, N. A nonlinear dynamic approach for evaluating postural control: new directions for the management of sport-related cerebral concussion. *Sports Med.* **35**, 935–950 (2005).

41. Stolarz, M., Żuk, M., Król, E. & Dziubińska, H. Circumnutation Tracker: novel software for investigation of circumnutation. *Plant Methods* **10**, 24. https://doi.org/10.1186/1746-4811-10-24 (2014).
42. Mottet, D. & Bootsma, R. J. The dynamics of goal-directed rhythmical aiming. *Biol. Cybern.* **80**, 234–245 (1999).
43. Stephen, D. G. & Dixon, J. A. The self-organization of insight: entropy and power laws in problem solving. *J. Probl. Solving* **2**, 72–101 (2009).
44. Costa, M., Peng, C.-K., Goldberger, A. L. & Hausdorff, J. M. Multiscale entropy analysis of human gait dynamics. *Phys. A* **330**, 53–60 (2003).
45. Kaplan, D. & Glass, L. *Understanding Nonlinear Dynamics* (Springer, Berlin, 1995).
46. Richman, J. S. & Moorman, J. R. Physiological time-series analysis using approximate entropy and sample entropy. *Am. J Physiol. Heart C* **278**, 2039–2049 (2000).
47. Costa, M., Goldberger, A. L. & Peng, C.-K. Multiscale entropy analysis of biological signals. *Phys. Rev. E* **71**, 021906. https://doi.org/10.3389/fncom.2015.00064 (2005).
48. Hu, M. & Liang, H. Intrinsic mode entropy based on multivariate empirical mode decomposition and its application to neural data analysis. *Cogn. Neurodynamics* **5**, 277–284 (2011).
49. Gao, J., Cao, Y., Tung, W.-W. & Hu, J. *Multiscale Analysis of Complex Time Series* (Wiley, New York, 2007).
50. Pincus, S. M. Approximate entropy as a measure of system complexity. *Proc. Natl. Acad. Sci. USA* **88**, 2297–2301 (1991).
51. Lake, D. E., Richman, J. S., Griffin, M. P. & Moorman, J. R. Sample entropy analysis of neonatal heart rate variability. *Am. J. Physiol. Reg. I* **283**, 789–797 (2002).
52. Ramdani, S., Seigle, B., Lagarde, J., Bouchara, F. & Bernard, P. L. On the use of sample entropy to analyze human postural sway data. *Med. Eng. Phys.* **31**, 1023–1031 (2009).
53. Costa, M., Goldberger, A. L. & Peng, C.-K. Multiscale entropy analysis of physiologic time series. *Phys. Rev. Lett.* **89**, 062102. https://doi.org/10.1103/PhysRevLett.89.068102 (2002).
54. Ahmed, M. U., Rehman, N., Looney, D., Rutkowski, T. M. & Mandic, D. P. Dynamic complexity of human responses: a multivariate data-adaptive framework. *B. Pol. Acad. Sci. Technol.* **60**, 433–445 (2012).
55. Hu, M. & Liang, H. Adaptive multiscale entropy analysis of multivariate neural data. *IEEE. Trans. Biomed. Eng.* **59**, 12–15 (2012).
56. Yentes, J. M. *et al.* The appropriate use of approximate entropy and sample entropy with short data sets. *Ann. Biomed. Eng.* **41**, 349–365 (2013).
57. Kuznetsov, N., Bonnette, S. & Riley, M. A. Nonlinear time series methods for analyzing behavioral sequences. In *Complex Systems in Sport* (eds Davis, K. *et al.*) 83–102 (Routledge, London, 2013).
58. Bruce, E. N. Measures of respiratory pattern variability. In *Bioengineering Approaches to Pulmonary Physiology and Medicine* (ed. Khoo, M. C. K.) 149–159 (Plenum Press, New York, 1996).
59. Zhang, Y.-C. Complexity and 1/*f* noise. A phase space approach. *J. Phys.* **I**(1), 971–977 (1991).
60. Acharya, U. R., Faust, O., Kannathal, N., Chua, T. L. & Laxminarayan, S. Non-linear analysis of EEG signals at various sleep stages. *Comput. Methods Prog Biol.* **80**, 37–45 (2005).
61. Eke, A. *et al.* Physiological time series: distinguishing fractal noises from motions. *Pflügers Archiv.* **439**, 403–415 (2000).
62. Takens, F. Detecting strange attractors in turbulence. In *Lecture Notes in Mathematics, Dynamical Systems and Turbulence* Vol. 898 (eds Rand, D. & Young, L.-S.) 366–381 (Springer, Berlin, 1981).
63. Volkov, A. G. *Plant Electrophysiology: Signaling and Responses* (Springer, Berlin, 2012).
64. Dickey, D. A. & Fuller, W. A. Distribution of the estimators for autoregressive time series with a unit root. *J Am. Stat. Assoc.* **74**, 427–431 (1979).
65. Depalo, D. A seasonal unit-root test with Stata. *Stata J.* **9**, 422–438 (2009).
66. Greene, W. H. *Econometric Analysis* (Prentice Hall, Upper Saddle River, 1997).
67. Franses, P. H. Seasonality, non-stationarity and the forecasting of monthly time series. *Int. J. Forecast.* **7**, 199–208 (1991).
68. Fernandez, L. & Bootsma, R. J. Effects of biomechanical and task constraints on the organization of movement in precision aiming. *Exp. Brain Res.* **159**, 458–466 (2004).
69. Kantz, H. & Schreiber, T. *Nonlinear Time Series Analysis* (Cambridge University Press, Cambridge, 2004).
70. Lake, D. E., Richman, J. S., Griffin, M. P. & Moorman, J. R. Sample entropy analysis of neonatal heart rate variability. *Am. J. Physiol.* **283**, 789–797 (2002).
71. Goldberger, A. *et al.* PhysioBank, PhysioToolkit, and PhysioNet: components of a new research resource for complex physiologic signals. *Circulation* **101**, e215–e220. https://doi.org/10.1161/01.cir.101.23.e215 (2000).
72. Costa, M., Ghiran, I., Peng, C.-K., Nicholson-Weller, A. & Goldberger, A. L. Complex dynamics of human red blood cell flickering: alterations with in vivo aging. *Phys. Rev. E.* **78**, 020901. https://doi.org/10.1103/PhysRevE.78.020901 (2008).
73. Hornero, R., Abasolo, D., Escudero, J. & Gomez, C. Nonlinear analysis of electroencephalogram and magnetoencephalogram recordings in patients with Alzheimer's disease. *Philos. Trans. R. Soc. A.* **367**, 317–336 (2009).
74. Valencia, J. F. *et al.* Refined multiscale entropy: application to 24-h holter recordings of heart period variability in healthy and aortic stenosis subjects. *IEEE. Trans. Biomed. Eng.* **56**, 2202–2213 (2009).
75. Rilling, G. & Flandrin, P. One or two frequencies? The empirical mode decomposition answers. *IEEE Trans. Signal Process.* **56**, 85–95 (2008).
76. Bates, D., Maechler, M., Bolker, B. & Walker, S. fitting linear mixed-effects models using lme4. *J. Stat. Softw.* **67**, 1–48 (2015).
77. R Core Team. *R: A language and environment for statistical computing. R Foundation for Statistical Computing*; https://www.r-project.org (2012).


## Acknowledgements

We are thankful to P. Adrian Frazier for his help in creating Figure 1 and in proofreading the manuscript, and to Krystyna B. Wieczerzak for her help in improving the rest of figures. Paco Calvo is supported by the *Office of Naval Research Global* (Award No. N62909-19-1-2015).

## Author contributions

V.R. and P.C. conceived the experiment. P.C. designed and built up the experimental setup. R.H. and P.C. run the experiments. V.R. and P.S. conceived the dynamical and statistical analyses. V.R. digitalized the data and performed the dynamical and statistical analyses. V.R., P.S., and P.C. wrote the manuscript.

## Competing interests

The authors declare no competing interests.

## Additional information

**Supplementary information** is available for this paper at https://doi.org/10.1038/s41598-020-76588-z.

**Correspondence** and requests for materials should be addressed to V.R.